Selective Electroreduction of Nitrate into Ammonia on CuCoAl Layered Double Hydroxide for Sustainable Resourcification

Wanying Wang,[a] Jiu Chen,[a] Edmund C. M. Tse [*,a]

[a] Department of Chemistry, CAS-HKU Joint Laboratory of Metallomics on Health and Environment, University of Hong Kong, Hong Kong SAR, China

Abstract

One-step nitrate electroreduction (NO_3RR) is a promising strategy to generate ammonia in a straightforward and environmentally friendly manner. However, most catalysts suffer from limited electrocatalytic activity as well as poor selectivity. In this work, a tunable trimetallic CuCoAl layered double hydroxide (LDH) catalyst was designed to generate ammonia exclusively and efficiently with an onset potential at 0.13 V vs. RHE. The synergy among Cu, Co, and Al bestowed a 99.5 % Faradaic efficiency (FE) for ammonia with a yield rate of 0.22 mol h^{-1} g^{-1}, rivaling the performance of state-of-the-art non-precious metal NO_3RR electrocatalysts. Control materials were employed to elucidate the roles of Cu, Co, and Al toward lowering the overpotential and suppressing the formation of nitrite byproduct. DFT calculations were performed to further investigate the adsorption strength of anionic adducts and electrolytes on LDH surface to unravel the effects of buffer conditions on NO_3RR performance. The scalable nature of our earth-abundant catalysts is particularly attractive due to the intrinsic low costs of

the raw materials. We envision that this precious-metal-free catalyst can be generally applicable to other resourcification processes to achieve a future sustainable society.

Introduction

Green production of value-added compounds via waste upcycling is key to realizing a sustainable society with efficient resourcification cycles.[1-3] Nitrate, a major contaminant in ground water, is typically discharged anthropogenically from nitrogen-containing fertilizers.[4] Excess nitrate accumulated in human bodies can be converted into carcinogenic *N*-nitroso species, leading to severe diseases such as methemoglobinemia.[5, 6]

To remove nitrate from wastewater, physical methods such as electrodialysis,[7] reverse osmosis,[8] and membrane filtration technologies[9] have been used. However, these methods only isolate, but not eliminate, nitrate from water. The trapped nitrate can then be treated via a heavily energy-intensive oxygenation step, followed by a bacterial denitrification step that requires special attention to maintain strict control over the dissolved oxygen, carbon sources, and pH of the biofilm reactors. In addition to the costly biological method, nitrate removal can be achieved via chemical reduction using hydrogen gas. However, due to the arduous production and transportation processes of hydrogen gas, this abiological method has limited usage in industrial settings. Therefore, electrocatalysis gradually becomes an alternative strategy.[10-13]

Toxic nitrate and nitrite hold the potential to be upcycled into other nitrogen-containing compounds, such as hydroxylamine and ammonia that show wide

applications in the pharmaceutical and agricultural industries.[14, 15] The traditional method to generate ammonia is through the Haber-Bosch process, which hydrogen and nitrogen gasses are mixed at 400-650 °C and pressurized to 200 atm for ammonia synthesis.[16] In addition to the harsh conditions required to break the N≡N bond, the production and purification of hydrogen gas in the first place is also energy intensive. To address the shortcomings of thermal N_2 reduction, a promising alternative strategy to convert nitrate into ammonia and other value-added products through electrochemical reduction was developed.[17-21] This electrocatalytic nitrate decomposition and removal process can proceed under ambient condition (N–O BDE: 204 kJ/mol) and bypass the energy-intensive N_2 breaking step in N_2 reduction (941 kJ/mol).[22-24]

Electrochemical reduction of nitrate to ammonia goes through an eight-electron pathway, where side reaction to generate other N-containing product or competitive hydrogen evolution can dominate, resulting in low Faradaic efficiency and product selectivity.[25-29] Lot of efforts have been invested to develop catalysts with high selectivity for desired products.[29-34] Noble metal such as Pt has been considered as a typical heterogeneous catalyst for nitrate reduction.[35-37] For non-precious metals, Cu is considered as a potential candidate for nitrate reduction to ammonia.[38-41] In 1 M KOH solution, Cu can reach a Faradaic efficiency of greater than 90 % for nitrate reduction into ammonia.[42] However, Cu tends to be deactivated due to cathodic corrosion in alkaline. In acidic solution, fresh Cu active sites can be regenerated through redeposition of leached Cu ions to allow for efficient nitrate reduction activity. Despite

Cu being an excellent catalyst for nitrate reduction to nitrite, two technological barriers remain to be tackled. First, Cu is easily deactivated during long-term operation.[43] Second, Cu is inefficient toward further downstream reduction of nitrite into other *N*-containing products.[23]

Two strategies have been demonstrated to enhance nitrate electroreduction activity and product selectivity. The first strategy is heteroatom alloying or doping.[44-47] With the addition of Ge to Pd, the bimetallic Pd-Ge catalyst can generate hydroxylamine with high selectivity.[48] The second strategy is nanostructure engineering.[49-53] The precise modification of catalysts could contribute to the enhanced catalytic activities.[54-57] Layered double hydroxide (LDH) with a lamellar structure shows high electrocatalytic activities toward oxygen evolution reaction (OER).[58-61] Combining these two strategies would afford a multi-metallic LDH with tremendous advantages such as an efficient synthetic procedure to achieve a stable nanostructure that allows for high-throughput composition screening to achieve a high-performance nitrate reduction catalyst.[62]

Herein, we developed a trimetallic CuCoAl LDH catalyst for nitrate electroreduction. Cu was selected because it exhibits a low overpotential toward nitrate reduction but displays a high yield rate for nitrite by-product, while Al was included to achieve the desired LDH structure. Co was chosen to test whether Co can enhance the ammonia yield rate. Together, this trio of metals reduces nitrate into ammonia with a high Faradaic efficiency (99.5 %) and a respectable ammonia yield rate (0.22 mol h^{-1} g^{-1}) in neutral condition. The roles and synergic effects of Cu, Co, and Al are further explored through electrochemical studies with control LDH materials to show that the

co-presence of Cu, Co, and Al is central to the overall nitrate reduction performance observed for the CuCoAl catalyst.

Experimental section

General Procedures. Copper nitrate trihydrate ($Cu(NO_3)_2 \cdot 3H_2O$, J&K Scientific), cobalt nitrate monohydrate ($Co(NO_3)_2 \cdot H_2O$, Alfa Aesar), aluminum nitrate nonahydrate ($Al(NO_3)_3 \cdot 9H_2O$, 3A Materials), sodium carbonate (Na_2CO_3, Dieckmann), sodium hydroxide (NaOH, A.R. Dieckmann), sodium sulfate (Na_2SO_4, Sigma-Aldrich), sodium hydrogen phosphate (Na_2HPO_4, Dieckmann), sodium dihydrogen phosphate (NaH_2PO_4, J&K Scientific), Nafion perfluorinated resin solution (5 wt% in lower aliphatic alcohols and water, containing 15-20% water, Sigma-Aldrich), potassium nitrate (KNO_3, Acros Organics), sodium nitrite ($NaNO_2$, Acros Organics), ammonium chloride (NH_4Cl, A.R. Dieckmann), phenol (C_6H_5OH, Sigma-Aldrich), sodium citrate anhydrous ($Na_3C_6H_5O_7$, J&K Scientific), sodium hypochlorite solution (NaClO solution, 11-14% available chlorine, Alfa Aesar), and sodium nitroprusside ($Na_2Fe(CN)_5 \cdot NO \cdot 2H_2O$, A.R. Beijing huagongchang) were purchased and used without further purification. Buffer solutions were prepared using Milli-Q water (>18 MΩ cm) and sparged with high-purity argon gas (Linde) for 30 min prior to each electrochemical experiment.

Preparation of CuCoAl LDH Electrocatalyst. CuCoAl LDH was prepared by coprecipitation.[63] $Co(NO_3)_2 \cdot H_2O$ (1.5 mmol), $Al(NO_3)_3 \cdot 9H_2O$ (0.5 mmol), and $Cu(NO_3)_2 \cdot 3H_2O$ (0.5 mmol) were dissolved in 10 mL Milli-Q water by sonication. A basic solution containing 0.05 M Na_2CO_3 and 0.2 M NaOH was added into the as-prepared metal salt solution dropwise with vigorous stirring until a pH 10 solution was

reached. The metal salt suspension was then aged at 90 ˚C for 6 h. The resulting solution was centrifuged, and the solid was collected and dried at 60 ˚C for 24 h in vacuo. The dried solid was grounded by mortar and pestle. CuCoAl LDH/Vulcan was prepared using the above synthesis procedure with the addition of Vulcan (50 mg) as substrate into the metal salt solution in the first step prior to slow addition of base. A catalyst ink was prepared following published protocols before electrochemical testing.[64] 10 mg CuCoAl LDH/Vulcan powder was suspended into 1 mL EtOH, and 6 μL Nafion perfluorinated resin solution was added with sonication for at least 15 min. 6 μL as-prepared ink was dropped onto a glassy carbon electrode (GC, diameter = 3 mm) and dried under a stream of N_2.

Characterization. X-ray diffraction (XRD) patterns were collected from an X-ray powder diffractometer (Bruker D8 Advance) with Cu Kα radiation at 40 kV and 40 mA and a LynxEye detector. The angle ranged from 5° to 80°, step size was 0.02, and time per step was 2 s. The sample morphology was examined using a scanning electron microscope (Hitachi S4800 FEG) and a scanning transmission electron microscope (FEI Tecnai G2 20 STWIN). Energy-dispersive X-ray spectroscopy (EDS) was conducted using a X-Max 80 EDS Detector. All the collected images were analyzed following a published method.[65] The sample composition was determined by X-ray photoelectron spectroscopy (XPS) using a X-ray photoelectron spectrometer microprobe (Thermo Scientific ESCALAB XI^+). All data were analyzed following a published protocol.[66, 67] The metal contents of the samples were quantified by inductively coupled plasma mass spectrometry (ICP-MS, Agilent Technologies 7700).

Electrochemical Measurements. Electrochemical measurements were conducted using a 660E electrochemical workstation (CH Instruments, Austin, TX) in a three-electrode H-type cell. GC modified with electrocatalyst, Ag/AgCl (3 M KCl), and Pt coil were used as working, reference, and counter electrodes, respectively. 0.5 M Na_2SO_4 and 0.5 M sodium phosphate buffer were prepared as electrolyte solutions. KNO_3 was added to the electrolyte solutions to achieve a final KNO_3 concentration of 50 mM. 4 mL of the final solution was added into the H-cell. Before electrochemical experiments, the solution was sparged with Ar, while the H-cell headspace was purged with Ar. Linear sweep voltammetry (LSV) was conducted at a scan rate of 10 mV s^{-1}. Electrolysis was performed at a given potential for a designated time interval. Two strategies were applied to analyze the stability of the LDH electrocatalysts. The first strategy held the same catalyst at one potential for 30 min, then the solution was replaced with a fresh one, and this cycle was repeated multiple times. The second strategy held the catalyst at a given potential for 32 h in a continuous fashion without changing the solution. All potentials reported were converted to RHE.

Product Analysis. Nitrate and nitrite concentrations were quantified by an ion chromatograph system (Thermo Scientific ICS-1100). Ammonia was quantified by an indophenol blue method.[68] The Faradaic efficiency was calculated using *Eq (1)*:

$$FE = \frac{n \times F \times c \times v}{Q} \times 100\% \quad Eq\ (1)$$

where n represents the number of electrons transferred during the electrochemical reaction, F is Faraday constant, c is the product molar concentration, v is the solution volume on the working electrode chamber during electrolysis, and Q is the total charge

passed. The yield rate of products was calculated using *Eq (2)*, using ammonia as example:

$$Yield_{NH_4^+} = \frac{Mole_{NH_4^+}}{m_{Cat.} \times t} \qquad Eq\ (2)$$

where $Mole_{NH_4^+}$ represents the mole of ammonia generated during electrolysis, $m_{Cat.}$ represents the total mass of the metal catalyst applied in each reaction, and t represents the reaction time.

Computational Method. All simulations were carried out using the Vienna *ab initio* simulation (VASP) package with the projector augmented wave (PAW).[69, 70] The Perdew-Burke-Ernzerhof (PBE) exchange-correlation functional of the generalized gradient approximation (GGA) method was used to describe the electron exchange correlation effects during VASP simulations,[71] and the values of the Hubbard-U parameter (U-J) were 3.60 eV for Cu and 3.52 eV for Co.[72, 73] The plane wave cutoff energy was 400 eV for valence electrons.

Brillouin zone integrations were performed with a 2×4×3 Gamma k-point mesh grid for bulk solids and a 3×3×1 Gamma k-point mesh grid for slabs. To avoid the interaction between two layers, the vacuum layer was set to 20 Å in the slab model and the bottom of the slab was fixed. The geometrical structures were determined by the convergence threshold value of force and energy less than 0.05 eV/Å and 1.0^{-4} eV, respectively.

The adsorption energy was defined as follows:

$$E_{ads} = E_{total} + E_{substrate} + E_{molecule} \qquad Eq\ (3)$$

in which E_{total} and E_{slab} were the total energy with and without adsorbate,

respectively, and $E_{molecule}$ was the energy of the molecule of interest.

Based on the 1:1:3 Cu:Al:Co ratio as well as the general formula of LDH ($[M^{2+}_{1-x}M^{3+}_{x}(OH)_2]^{x+}(CO_3^{n-})_{x/n}$) with x=n=0.2, a LDH model with a $R\bar{3}m$ point group was constructed by partially replacing Co in CoOOH with Cu and Al. The lattice parameters were optimized as 13.75, 6.35, and 10.76 Å, and two unit cells were used in computational studies.

Results and discussion

Synthesis and Characterization of Non-Precious Layered Double Hydroxides

Non-precious CuCoAl LDH is synthesized through a scalable co-precipitation method using nitrate salts of Cu, Co, and Al (**Error! Reference source not found.**). These earth-abundant metals are chosen because Cu is active toward overcoming the rate-determining step of nitrate-to-nitrite conversion and Al is conducive toward LDH formation. The hypothesis of this study is to test if Co can facilitate downstream nitrite-to-ammonia reduction. For pristine LDH samples, upon tuning the aqueous mixture to slightly basic pH and aging at elevated temperatures, brown precipitates are isolated by centrifugation and used without further purification. For carbon-supported samples, mesoporous Vulcan carbon is introduced to the aqueous mixture prior to the nucleation step. The layered nanomaterials gradually precipitate on the carbon surface in the alkali medium to form CuCoAl LDH/Vulcan.

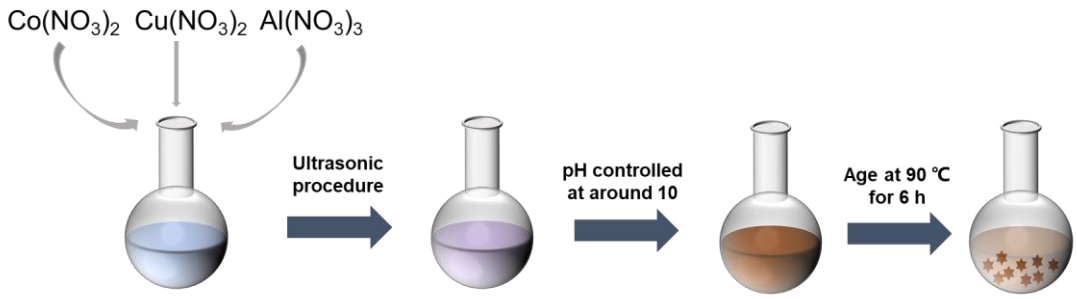

Fig. 1 Schematic illustrating the synthesis of CuCoAl LDH.

The morphology and crystallinity of the as-synthesized CuCoAl LDH are characterized using scanning electron microscopy (SEM), transmission electron microscopy (TEM), and X-ray diffraction (XRD). XRD data show that the CuCoAl LDH diffraction pattern is consistent with the characteristic peaks of a hydrotalcite-like phase (JCPDS: 41-1428) (**Error! Reference source not found.**a).[74] The introduction of Vulcan to CuCoAl LDH does not impact the crystal phases observable for the CuCoAl LDH/Vulcan composite using XRD (Fig. S1). SEM and TEM show that CuCoAl LDH displays a hexagonal flake-like structure. High-resolution TEM further reveals that the CuCoAl LDH crystallite exhibits a lamellar structure with a lattice spacing of 0.66 nm (Fig. 2b-d), which is correlated with the (001) plane detected by XRD. For the CuCoAl LDH/Vulcan composite, sheet-like CuCoAl LDH uniformly decorates the amorphous Vulcan surface, demonstrating good cohesion between the multi-metallic catalyst and the carbon substrate. More importantly, the introduction of Vulcan shows no impact on the CuCoAl LDH morphology (Fig. S2).

The chemical composition and metal distribution of the as-synthesized CuCoAl LDH are characterized using XPS, EDS, and ICP-MS. XPS data show that Cu, Co, and Al are present in the nanoplates (**Error! Reference source not found.**e-h, Fig. S3).

High-resolution XPS shows that Cu^{2+}, Co^{2+}, and Al^{3+} are present in the as-synthesized catalyst. After the incorporation of Vulcan, the binding energies of Co^{2+} and Cu^{2+} shift to higher values by ca. 1.5 eV, suggestive of a change in the chemical microenvironments surrounding the metal ions.[75]

EDS mapping shows that metal ions are well-dispersed on the Vulcan carbon substrate (Fig. S4). ICP-MS quantification shows that 5.23 mg Cu, 13.5 mg Co, and 2.18 mg Al are dropcasted onto a GC electrode for electrochemical studies (Fig. S5). The Cu:Co:Al ratio in the LDH catalyst is quantified to be 1:3:1 by EDS and ICP-MS. This empirical Cu:Co:Al ratio is consistent with the feed ratio used in the preparation of CuCoAl LDH (Table S1). These materials characterization efforts collectively demonstrate the successful preparation of CuCoAl LDH on Vulcan.

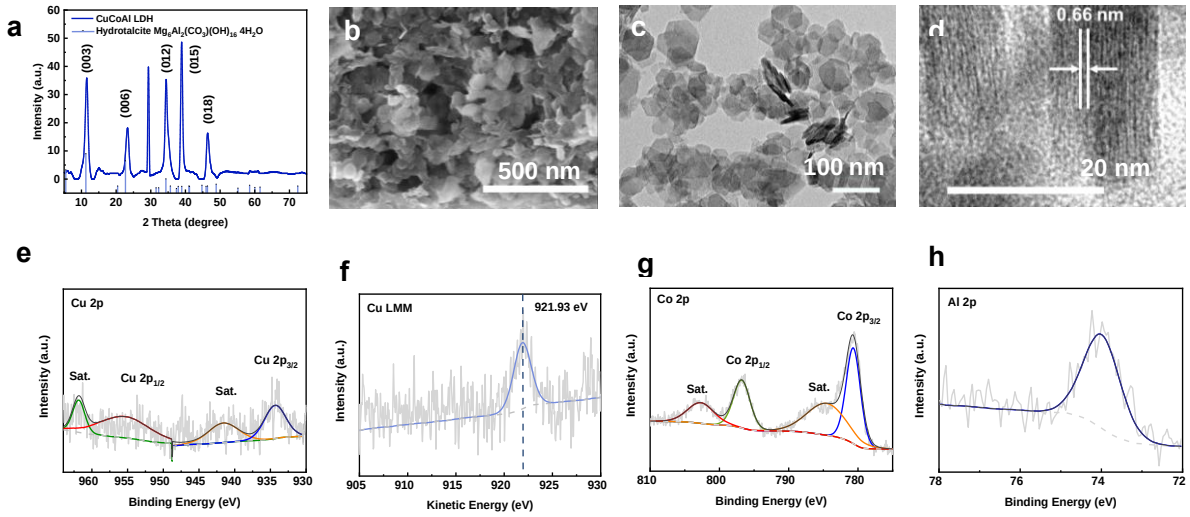

Fig. 2 Materials characterization of CuCoAl LDH. (a) XRD pattern; (b) SEM image; (c, d) TEM image; (e-h) XPS data: (e) Cu 2p; (f) Cu LMM; (g) Co 2p; (h) Al 2p.

Electrocatalytic Nitrate Reduction Activity and Product Selectivity of CuCoAl LDH

The electrocatalytic nitrate reduction performance of CuCoAl LDH is next

examined using linear sweep voltammetry (LSV). In the absence of nitrate, CuCoAl LDH/Vulcan catalyzes the hydrogen evolution reaction (HER) with an onset potential of -0.5 V vs. RHE (**Error! Reference source not found.**a, red dashed line). Upon the addition of nitrate to the phosphate buffer, the magnitude of the cathodic current density increases drastically, indicating that nitrate is reduced by CuCoAl LDH/Vulcan (**Error! Reference source not found.**a, red solid line). Vulcan-only and GC electrode are used as controls to probe the background reduction current density in the absence of CuCoAl LDH/Vulcan. **Error! Reference source not found.**a shows that the reduction current density of CuCoAl LDH/Vulcan in the presence of nitrate far exceeds those of Vulcan-only (green) and GC electrode (blue). Together, these results show that CuCoAl

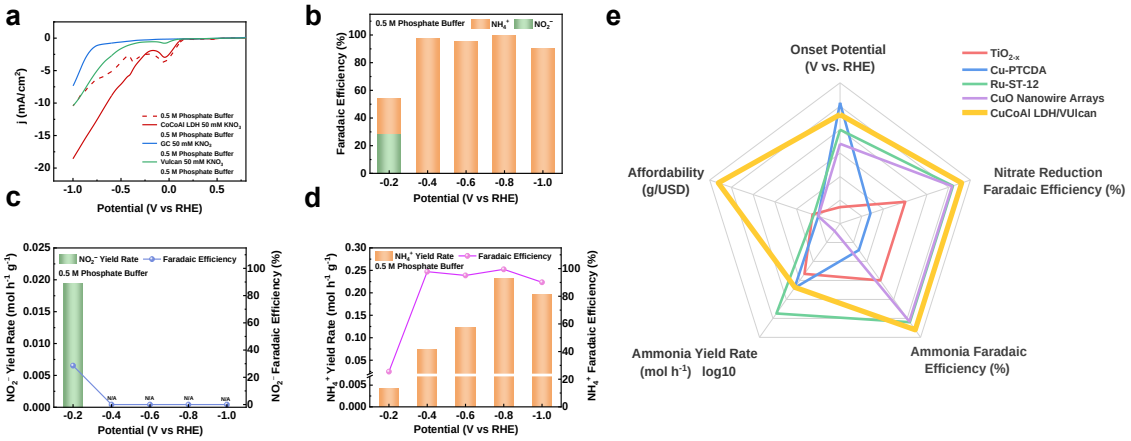

Fig. 3 (a) LSV curves of GC electrode (blue), Vulcan-only (green), and CuCoAl LDH/Vulcan (red) with (solid line) and without (dashed line) nitrate addition in 0.5 M phosphate buffer; (b) Faradaic efficiency of nitrate reduction at designated potential; (c-d) Nitrite/ammonia yield rate and its Faradaic efficiency at designated potential. (e) Comparison of CuCoAl LDH with other state-of-the-art catalysts in terms of nitrate reduction catalytic performance.

LDH/Vulcan is an efficient nitrate reduction catalyst.

Next, nitrate reduction product selectivity is assessed by subjecting CuCoAl LDH/Vulcan to a constant potential treatment. Nitrite and ammonia, two nitrate

reduction products, are quantified using ion chromatography (IC) and a colorimetric assay based on indophenol blue, respectively (Fig. S6). At -0.2 V, CuCoAl LDH/Vulcan displays a similar Faradaic efficiency (FE) of ca. 22 % for both nitrite and ammonia production (**Error! Reference source not found.**b). This result indicates that at this low overpotential nitrate reduction is incomplete and inefficient. Interestingly, nitrite is only detected at -0.2 V but not at more negative potentials tested in this study (**Error! Reference source not found.**c), suggesting that nitrate reduction to ammonia becomes more favorable at higher overpotentials. Upon increasing the electrochemical driving force, the FE toward ammonia gradually increases to 99.5 % at -0.8 V, along with the yield rate reaching up to 0.22 mol h^{-1} g^{-1}, the highest yield rate achievable with CuCoAl LDH/Vulcan (**Error! Reference source not found.**d). The nitrate reduction electrocatalytic performance achieved by CuCoAl LDH/Vulcan surpasses most existing catalysts (Table S2). At -1.0 V, the overall nitrate reduction FE decreases slightly, which can be attributed to the presence of HER as a competing process. Taken together, these electrochemical studies show that CuCoAl LDH/Vulcan can upcycle toxic nitrate into value-added ammonia exclusively. This CuCoAl LDH has outcompeted state-of-the-art materials in terms of catalytic nitrate electroreduction performance ranging from activity and selectivity to durability and scalability (**Error! Reference source not found.**e).

Stability of CuCoAl LDH under Long-term Operating Condition for Nitrate Reduction

To assess the durability of CuCoAl LDH/Vulcan, the FE and yield rate of nitrate

reduction are monitored over 10 cycles with each cycle lasting 30 min. The overall FE of nitrate reduction catalyzed by CuCoAl LDH/Vulcan remains at >99 % without fading across 10 consecutive cycles at -0.4 V (**Error! Reference source not found.**a). Intriguingly, the yield rate and FE for ammonia maintains at levels above 0.08 mol h^{-1} g^{-1} and >95 % (**Error! Reference source not found.**b), along with the yield rate and

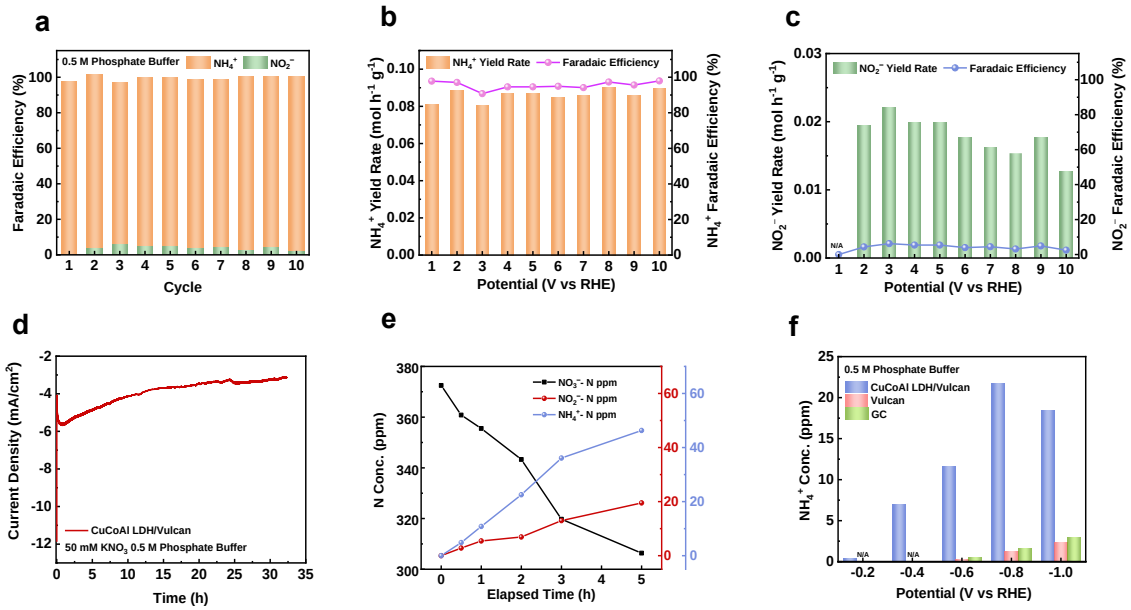

Fig. 4 (a-c) Nitrate reduction catalytic performance across 10 consecutive electrolysis runs in 0.5 M phosphorate buffer: (a) Nitrate reduction Faradaic efficiency; (b) Ammonia yield rate and Faradaic efficiency; (c) Nitrite yield rate and Faradaic efficiency; (d) Nitrate reduction long-term electrolysis curve; (e) Time-dependence test of nitrate, nitrite and ammonia concentration catalyzed by CuCoAl LDH at -0.4 V; (f) Nitrate reduction catalytic performance by CuCoAl LDH/Vulcan, Vulcan, and GC electrode at designated potential.

FE for byproduct nitrite below 0.02 mol h^{-1} g^{-1} and <5 % (**Error! Reference source not found.**c). SEM image shown in Fig. S7 demonstrates that CuCoAl LDH/Vulcan still retains its lamellar structure after 10 electrolysis cycles. These data together corroborate that CuCoAl LDH is a robust catalyst for reduction of nitrate into ammonia exclusively.

Chronoamperometry is conducted to obtain further evidence on the long-term stability of CuCoAl LDH/Vulcan under practical operating condition. Upon holding the catalyst at -0.4 V for 32 h, the magnitude of the nitrate reduction current density decreases gradually (**Error! Reference source not found.**d). The change in solution species concentration is then determined to understand the observed trend. IC and colorimetric assay show that nitrate concentration decreases continuously, while the concentration of ammonia and nitrite increases progressively (**Error! Reference source not found.**e). These quantification results suggest that the decrease in nitrate reduction activity originates from the consumption of nitrate. Vulcan-only and GC electrode are utilized as controls to validate the ability of CuCoAl LDH/Vulcan at converting nitrate into ammonia and nitrite. **Error! Reference source not found.**f shows that the amount of ammonia generated by CuCoAl LDH/Vulcan far exceeds Vulcan-only and GC electrode, verifying that CuCoAl LDH/Vulcan is an excellent catalyst for nitrate-to-ammonia valorization.

Electrolyte Effect on the Electrocatalytic Nitrate Reduction Performance of CuCoAl LDH

Next, the effect of electrolyte on the nitrate reduction performance of CuCoAl LDH/Vulcan is explored (Fig. S8). Electrolytes exhibit a significant impact on the catalytic nitrate reduction efficiency.[76] The nitrate reduction onset potential of CuCoAl LDH/Vulcan in phosphate buffer (Fig. S8a green) is 0.13 V, which is 130 mV more positive relative to that observed in Na_2SO_4 solution (Fig. S8a blue: 0 V), suggesting that CuCoAl LDH/Vulcan can reduce nitrate more readily in phosphate buffer than in

Na_2SO_4 solution.

Interestingly, the total cathodic current density observed in phosphate buffer is 15 mA/cm^2, which is 5 mA/cm^2 less than that recorded in Na_2SO_4 solution (20 mA/cm^2). A larger cathodic current may not necessarily translate into a higher nitrate reduction activity, because the extra cathodic current could originate from more background HER activity. GC quantification shows that more H_2 gas is evolved in Na_2SO_4 solution than in phosphate buffer at -1.0 V, suggesting that CuCoAl LDH/Vulcan is less selective for nitrate reduction in Na_2SO_4 solution than in phosphate buffer (Fig. S9). The total FE for nitrate reduction by CuCoAl LDH/Vulcan in phosphate buffer can approach up to 100 % at potentials more negative than -0.4 V and is higher than that achievable in Na_2SO_4 solution (Fig. S8b), further demonstrating that phosphate buffer suppresses background HER to a higher extent than Na_2SO_4 solution. Taken together, the identity of the electrolyte plays an important role in dictating the overall catalytic activity of CuCoAl LDH/Vulcan toward nitrate reduction. Specifically, the use of phosphate buffer promotes nitrate reduction and suppresses HER simultaneously on CuCoAl

LDH/Vulcan.

Maximizing the generation of desired ammonia product while minimizing the formation of nitrite byproduct is key to developing a selective nitrate reduction catalyst. **Error! Reference source not found.**, S8-10 show the impact of electrolyte solutions on the nitrate reduction product selectivity of CuCoAl LDH. At -0.8 V, CuCoAl LDH exhibits higher selectivity toward ammonia in phosphate buffer (**Error! Reference source not found.** green: 0.22 mol h^{-1} g^{-1} yield rate and 99.5 % FE at -0.8 V) than in Na_2SO_4 solution (**Error! Reference source not found.** blue: 0.15 mol h^{-1} g^{-1} yield rate and 89.4 % FE at -0.8 V). For byproduct generation, nitrite is only detected at -0.2 V in phosphate buffer with a yield rate of 0.019 mol h^{-1} g^{-1} and an FE of 28.5 % (Fig. S8e, f

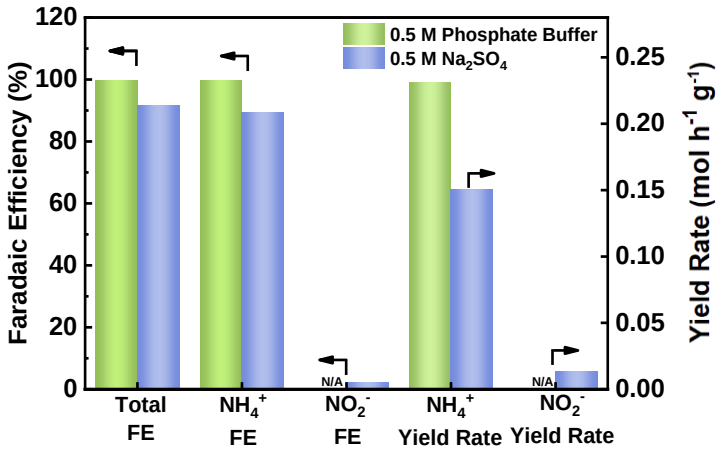

Fig. 5 Comparison of nitrate reduction Faradaic efficiency, ammonia Faradaic efficiency, nitrite Faradaic efficiency, ammonia yield rate, and nitrite yield rate between 0.5 M phosphate buffer and 0.5 M Na_2SO_4 solution at -0.8 V.

green), while nitrite can be observed at all potentials except -1.0 V in Na_2SO_4 solution (Fig. S8e, f blue). These results corroborate that CuCoAl LDH/Vulcan is an efficient nitrate reduction catalyst with higher yield rate and higher FE for ammonia, along with lower yield rate and lower FE for nitrite, in phosphate buffer than in Na_2SO_4 solution.

DFT calculations are performed to examine the effect of electrolyte adsorption on

nitrate reduction. The optimal adsorption structures of NO_3^-, HPO_4^{2-}, $H_2PO_4^-$, and SO_4^{2-} on simulated CuCoAl LDH surfaces are shown in **Error! Reference source not found.**. The adsorption energy of NO_3^-, HPO_4^{2-}, $H_2PO_4^-$, and SO_4^{2-} are computed to be -2.95, -5.15, -3.84, and -4.50 eV, respectively. A more negative binding energy indicates a stronger interaction between the adsorbates and the LDH surface. Since the experiments are conducted at neutral pH, the average adsorption strength of phosphate species with a pK_a of 7.2 is calculated to be -4.50 eV, which is similar to that of SO_4^{2-}. Since sulfate and phosphate species share similar computed binding strengths on LDH surfaces, the preferences of anionic species for adsorption sites on LDH surfaces are explored as the origin for the differences in onset potential observed. The adsorption site with the lowest energy value calculated is taken as the preferred binding site of the anion of interest. Intriguingly, NO_3^- and SO_4^{2-} share the same adsorption site on LDH (**Error! Reference source not found.**a,b) while the phosphate species prefer a different site (**Error! Reference source not found.**c,d). Since NO_3^- and SO_4^{2-} bind to the same site on LDH, SO_4^{2-} is anticipated to impact the binding of NO_3^-. Together with the computed adsorption energies that NO_3^- (-2.95 eV) binds stronger to LDH than SO_4^{2-} (-4.50 eV), Na_2SO_4 electrolyte is expected to inhibit nitrate adsorption and hinder subsequent nitrate reduction. On the other hand, since phosphate species and nitrate bind to different sites, phosphate species have less influence on nitrate binding and further reduction. Taken together, the computational results suggest that Na_2SO_4 electrolyte has a higher negative impact on the nitrate reduction efficiency, which is consistent with the experimental observation that the nitrate reduction overpotential is

lowered by 130 mV upon switching from Na_2SO_4 to phosphate buffer (**Error! Reference source not found.**).

The electrolyte identity can also play a role in determining the stability of CuCoAl LDH/Vulcan during nitrate reduction. A stability test in Na_2SO_4 solution is conducted in a fashion analogous to that in phosphate buffer (Fig. S10). The overall FE of CuCoAl LDH/Vulcan decreases continuously during electrolysis at -0.4 V in Na_2SO_4 solution (Fig. S10a). Compared with phosphate buffer, less ammonia and more nitrite are generated in Na_2SO_4 solution (Fig. S10b, c). During the course of electrolysis, H_2 is

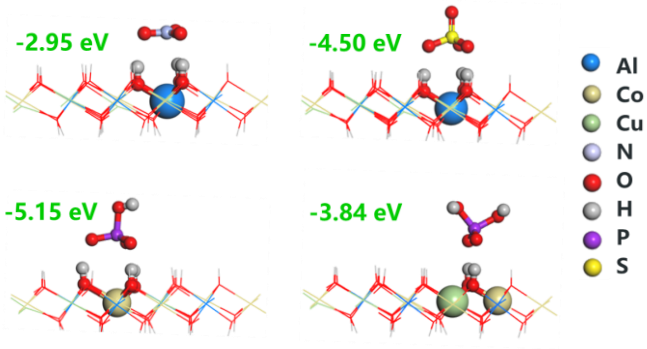

Fig. 6 The adsorption structure of (a) NO_3^-, (b) SO_4^{2-}, (c) HPO_4^{2-}, and (d) $H_2PO_4^-$. Numbers in green refer to the adsorption energy of anionic species on the surface of CuCoAl LDH.

detected though GC. These observations suggest that HER competes with nitrate reduction and ultimately corrupts the integrity of the catalyst, matching phenomena observed in previous studies.[77] The presence of HER can further explain the high cathodic current density observed in the LSV recorded in Na_2SO_4 solution (Fig. S8a blue). This comparative stability test shows that CuCoAl LDH/Vulcan is more robust in phosphate buffer than in Na_2SO_4 solution.

Considering the nitrate reduction onset potential, ammonia yield rate and FE, and nitrite byproduct generation, phosphate buffer is an excellent choice for nitrate

reduction by CuCoAl LDH/Vulcan. Vulcan-only and GC electrode control results show that the identity of the electrolyte does not impact their nitrate reduction performance (Fig. S11), further confirming that the differences in nitrate reduction performance observed originate from the interaction between the electrolyte and CuCoAl LDH/Vulcan. The versatility of CuCoAl LDH/Vulcan to conduct nitrate reduction with high utility in a wide variety of electrolyte conditions has direct implications in wastewater treatment where excess nitrate, phosphate, and sulfate are found together in agricultural, municipal, and industrial waste streams.

Synergistic Effects of Cu, Co, and Al in LDH Catalysts for Nitrate Reduction

To investigate the origin of the outstanding nitrate reduction performance of CuCoAl LDH, two controls (CuAl LDH and CoAl LDH) are synthesized to gain insights into the function of each metal. Fig. S12 shows the XRD spectra of CuAl LDH/Vulcan and CoAl LDH/Vulcan, where their XRD patterns correspond to a hydrotalcite structure. Fig. S13 and S14 show the SEM and TEM images of CuAl LDH and CoAl LDH. CuAl LDH exhibits a flower-like structure (Fig. S13), while CoAl LDH displays a plate-like morphology similar to CuCoAl LDH (Fig. S14). XPS data further reveal the presence of Cu^{2+} and Al^{3+} ions in CuAl LDH (Fig. S15) and the presence of Co^{2+} and Al^{3+} ions in CoAl LDH (Fig. S16). These characterization studies confirm that CuAl LDH and CoAl LDH can serve as comparative models of CuCoAl LDH in subsequent electrochemical investigations.

The catalytic nitrate reduction performance of CuAl LDH and CoAl LDH is then interrogated. **Error! Reference source not found.**a shows the nitrate reduction LSVs

of CuAl LDH, CoAl LDH, and CuCoAl LDH. Among them, CuCoAl LDH (blue) and CuAl LDH (red) exhibit an onset potential at 0.13 V, which is more positive than the onset potential at -0.3 V displayed by CoAl LDH (green). **Error! Reference source not found.**b shows the total FE for nitrate reduction of the three catalysts. CuCoAl LDH (blue) and CoAl LDH (green) display FE toward nitrate reduction about 20% higher than CuAl LDH (red). In terms of ammonia production, CuCoAl LDH exhibits the highest ammonia yield rate from -0.4 to -0.8 V, while CoAl LDH displays the highest ammonia yield rate at -1.0 V (**Error! Reference source not found.**c). With regard to product selectivity, CuCoAl LDH shows the highest ammonia FE while CuAl LDH shows the lowest FE at all applied potentials (**Error! Reference source not found.**d). Considering the nitrite production, CuAl LDH demonstrates the highest nitrite Faradaic efficiency and yield rate. The introduction of Co lowers the byproduct nitrite generation (**Error! Reference source not found.**e, f). Collectively, these trends demonstrate that CuCoAl LDH displays nitrate reduction performance more superior than CuAl LDH and CoAl LDH (**Error! Reference source not found.**).

First, the role of Cu can be revealed by comparing CuCoAl LDH and CoAl LDH. The incorporation of Cu lowers the overpotential by 0.43 V to jumpstart nitrate reduction by promoting the initial two-electron transfer process to generate nitrite from nitrate (**Error! Reference source not found.**a). Similar onset potential enhancement can be observed in Na_2SO_4 solution (Fig. S17), further demonstrating that Cu

contributes significantly toward the improvement of the nitrate reduction onset potential.

Second, the role of Co can be unravelled by comparing CuCoAl LDH and CuAl

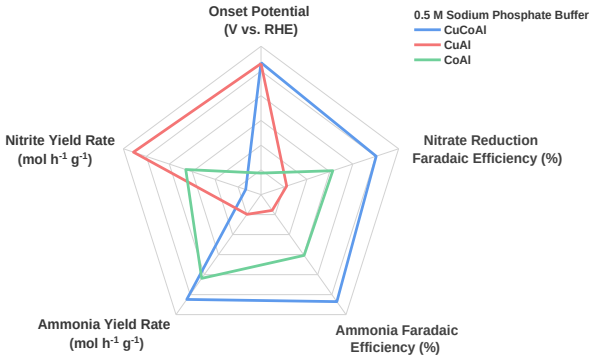

Fig. 8 Radar plot of the nitrate reduction performance of multimetallic LDH catalysts at -0.8 V.

LDH. The presence of Co increases FE by 2 folds and boosts ammonia yield rate at -0.4 V by 2 times (**Error! Reference source not found.**c, d). More importantly, the introduction of Co into the LDH structure generates ammonia exclusively with a FE of close to 100 % while suppressing byproduct nitrite production completely with a FE of close to 0 % at all potentials studied except at -0.2 V (**Error! Reference source not found.**e, f). Therefore, the incorporation of Co can eliminate toxic nitrite emission on CuCoAl LDH by facilitating downstream reduction of quasi-stable nitrite intermediate to further generate ammonia exclusively as the desired value-added product. These comparative studies show that both Cu and Co play important roles in determining and improving the overall nitrate reduction performance of LDH in a synergistic fashion.

Conclusions

Nitrate-to-ammonia upcycling powered by sustainable electricity is key to realizing a green society. At present, widespread adoption of the electroreduction strategy is

limited by the activity, selectivity, and scalability of the catalysts, which are typically composed of precious metals. Here, non-precious metal (NPM) layered double hydroxides (LDHs) were prepared via a one-pot precipitation method. A trimetallic LDH featuring Cu, Co, and Al was found to exhibit excellent electrocatalytic performance toward nitrate reduction with an onset potential at 0.13 V vs. RHE while generating ammonia exclusively with an outstanding Faradaic efficiency (FE) for ammonia reaching 99.5 % and a yield rate of 0.22 mol h^{-1} g^{-1}, rivalling the performance of state-of-the-art NPM nitrate reduction catalysts. The roles of Co and Cu toward imbuing LDH with high activity and selectivity were further investigated. The incorporation of Co resulted in a 2-fold increase in FE for ammonia as well as a 2-fold increase in ammonia yield rate at -0.4 V, indicating that Co is key to suppressing byproduct nitrite emission and subsequently enhancing the selectivity for ammonia production. The presence of Cu resulted in a positive shift of the nitrate reduction onset potential by 0.43 V, corroborating that Cu is instrumental toward lowering the electrochemical activation barrier and subsequently jumpstarting the nitrate upcycling process. Beyond boosting the overall efficiency and selectivity, the Cu-Co-Al synergy further endows this LDH with enhanced durability under operating conditions. Taken together, this work provides a promising strategy to design nanoscale earth-abundant electrocatalysts for nitrate-to-ammonia conversion with potential implications in industrial wastewater treatment as well as waste-to-commodity upcycling.

Conflicts of interest

The authors declare no competing financial interests.

Acknowledgements

E.C.M.T. would like to express gratitude to the National Natural Science Foundation of China for providing a Young Scientists Fund (NSFC: 22002132) on green catalysis and sustainable nanomaterials. W.W. was supported by a Hui Pun Hing Memorial Postgraduate Scholarship and the Shenzhen Science and Technology Innovation Commission Basic Science General Program (SZSTI: JCYJ20210324122011031). The authors would like to recognize Frankie Y.F. Chan at the Electron Microscope Unit (EMU) at the University of Hong Kong (HKU) for his help with nanomaterials characterization. The authors were grateful to Shengshou Ma and Prof. Kaimin Shih for their help with XRD measurements. This project is made possible through the initial support from the Woo Ting Sang Agricultural Development Research Fund (WTS: 263660516). The authors thank the Research Grants Council in Hong Kong for an EU–HK Research and Innovation Cooperation Co-funding Mechanism (RGC: E-HKU704/19), a Theme-based Research Scheme (TRS: T23-713/22-R), Research Matching Grant Schemes (RMGS: 207301212, 207301251), and an Early Career Scheme (RGC: 27301120) for expanding the electrochemical investigation capability as well as upgrading the nanomaterials characterization instruments at the HKU-CAS Joint Laboratory on New Materials.

References

1. F. Liu, X. Gao, R. Shi, C. Edmund and Y. Chen, *Green Chem.*, 2022, **24**, 6571-6577.
2. K.-J. Wu, C. Edmund, C. Shang and Z. Guo, *Prog. Mater Sci.*, 2022, **123**, 100821.
3. Z. Xu, F. Pan, M. Sun, J. Xu, N. E. Munyaneza, Z. L. Croft, G. Cai and G. Liu, *Proceedings of the National Academy of Sciences*, 2022, **119**, e2203346119.
4. A. Menció i Domingo, J. Mas-Pla, N. Otero Pérez, O. Regàs, M. Boy Roura, R. Puig i Caminal, J. Bach i Plaza, C. Domènech, M. Zamorano Cáceres and D. Brusi i Belmonte, © *Science of the Total Environment, 2016, vol. 539, p. 241-251*, 2016.
5. J. P. Van Der Hoek and A. Klapwijk, *Water Res.*, 1987, **21**, 989-997.
6. S. Li, J. Liang, P. Wei, Q. Liu, L. Xie, Y. Luo and X. Sun, *eScience*, 2022, **2**, 382-388.
7. A. El Midaoui, F. Elhannouni, M. Taky, L. Chay, M. A. M. Sahli, L. Echihabi and M. Hafsi, *Sep. Purif. Technol.*, 2002, **29**, 235-244.
8. A. Kapoor and T. Viraraghavan, *J. Environ. Eng.*, 1997, **123**, 371-380.
9. S. Samatya, N. Kabay, Ü. Yüksel, M. Arda and M. Yüksel, *React. Funct. Polym.*, 2006, **66**, 1206-1214.
10. J. Cavin, A. Ahmadiparidari, L. Majidi, A. S. Thind, S. N. Misal, A. Prajapati, Z. Hemmat, S. Rastegar, A. Beukelman and M. R. Singh.
11. M. Elmaalouf, M. Odziomek, S. Duran, M. Gayrard, M. Bahri, C. Tard, A. Zitolo, B. Lassalle-Kaiser, J.-Y. Piquemal and O. Ersen, *Nat. Commun.*, 2021, **12**, 1-10.
12. H. Cao, Z. Zheng, P. Norby, X. Xiao and S. Mossin, *Small*, 2021, **17**, 2100558.
13. Z. Liu, F. Zheng, W. Xiong, X. Li, A. Yuan and H. Pang, *SmartMat*, 2021, **2**, 488-518.
14. F.-Y. Chen, Z.-Y. Wu, S. Gupta, D. J. Rivera, S. V. Lambeets, S. Pecaut, J. Y. T. Kim, P. Zhu, Y. Z. Finfrock and D. M. Meira, *Nat. Nanotechnol.*, 2022, 1-9.
15. J.-X. Liu, D. Richards, N. Singh and B. R. Goldsmith, *ACS Catal.*, 2019, **9**, 7052-7064.
16. J. G. Chen, R. M. Crooks, L. C. Seefeldt, K. L. Bren, R. M. Bullock, M. Y. Darensbourg, P. L. Holland, B. Hoffman, M. J. Janik and A. K. Jones, *Science*, 2018, **360**, eaar6611.
17. W. He, J. Zhang, S. Dieckhöfer, S. Varhade, A. C. Brix, A. Lielpetere, S. Seisel, J. R. Junqueira and W. Schuhmann, *Nat. Commun.*, 2022, **13**, 1-13.
18. O. Q. Carvalho, R. Marks, H. K. Nguyen, M. E. Vitale-Sullivan, S. C. Martinez, L. Arnadottir and K. A. Stoerzinger, 2022.
19. Z. Wang, D. Richards and N. Singh, *Catal. Sci. Technol.*, 2021, **11**, 705-725.
20. H. Liu, J. Park, Y. Chen, Y. Qiu, Y. Cheng, K. Srivastava, S. Gu, B. H. Shanks, L. T. Roling and W. Li, *ACS Catal.*, 2021, **11**, 8431-8442.
21. Z.-Y. Wu, M. Karamad, X. Yong, Q. Huang, D. A. Cullen, P. Zhu, C. Xia, Q. Xiao, M. Shakouri and F.-Y. Chen, *Nat. Commun.*, 2021, **12**, 1-10.
22. Z. W. Seh, J. Kibsgaard, C. F. Dickens, I. Chorkendorff, J. K. Nørskov and T. F. Jaramillo, *Science*, 2017, **355**, eaad4998.
23. V. Rosca, M. Duca, M. T. de Groot and M. T. Koper, *Chem. Rev.*, 2009, **109**, 2209-2244.
24. H. Hirakawa, M. Hashimoto, Y. Shiraishi and T. Hirai, *ACS Catal.*, 2017, **7**, 3713-3720.
25. J. Li, G. Zhan, J. Yang, F. Quan, C. Mao, Y. Liu, B. Wang, F. Lei, L. Li, A. W. M. Chan, L. Xu, Y. Shi, Y. Du, W. Hao, P. K. Wong, J. Wang, S. X. Dou, L. Zhang and J. C. Yu, *J Am Chem Soc*, 2020, **142**, 7036-7046.
26. X. Mo, X. Gao, A. V. Gillado, H.-Y. Chen, Y. Chen, Z. Guo, H.-L. Wu and E. C. Tse, *ACS Nano*, 2022, **16**, 12202-12213.
27. T. Zeng, H.-L. Wu, Y. Li, C. Edmund and C. J. Barile, *Electrochim. Acta*, 2019, **320**, 134611.

28. W. Wang and E. C. Tse, *Inorg. Chem.*, 2021, **60**, 6900-6910.
29. T. Zeng, R. P. Gautam, D. H. Ko, H.-L. Wu, A. Hosseini, Y. Li, C. J. Barile and E. Tse, *Nat. Rev. Chem.*, 2022, 1-19.
30. T. Zeng, R. P. Gautam, C. J. Barile, Y. Li and E. C. Tse, *ACS Catal.*, 2020, **10**, 13149-13155.
31. Z. Wei, W. Wang, W. Li, X. Bai, J. Zhao, E. C. Tse, D. L. Phillips and Y. Zhu, *Angew. Chem. Int. Ed.*, 2021, **60**, 8236-8242.
32. L. C. Meyer, U. Sanyal, K. A. Stoerzinger, K. Koh, J. L. Fulton, D. M. Camaioni, O. Y. Gutiérrez and J. A. Lercher, *ACS Catal.*, 2022, **12**, 11910-11917.
33. M. Elmaalouf, A. Da Silva, S. Duran, C. Tard, M. Comesaña-Hermo, S. Gam-Derouich, V. Briois, D. Alloyeau, M. Giraud and J.-Y. Piquemal, *Chem. Sci.*, 2022, **13**, 11807-11816.
34. C. J. Barile, C. Edmund, Y. Li, J. P. Gewargis, N. A. Kirchschlager, S. C. Zimmerman and A. A. Gewirth, *Biophys. J.*, 2016, **110**, 2451-2462.
35. K. Nishimura, K. Machida and M. Enyo, *Electrochim. Acta*, 1991, **36**, 877-880.
36. G. Horanyi and E. Rizmayer, *J. Electroanal. Chem. Interfacial Electrochem.*, 1982, **140**, 347-366.
37. O. A. Petrii and T. Y. Safonova, *J. Electroanal. Chem.*, 1992, **331**, 897-912.
38. Y. Wang, W. Zhou, R. Jia, Y. Yu and B. Zhang, *Angew Chem Int Ed Engl*, 2020, **59**, 5350-5354.
39. G.-F. Chen, Y. Yuan, H. Jiang, S.-Y. Ren, L.-X. Ding, L. Ma, T. Wu, J. Lu and H. Wang, *Nat. Energy*, 2020, **5**, 605-613.
40. R. Daiyan, T. Tran-Phu, P. Kumar, K. Iputera, Z. Tong, J. Leverett, M. H. A. Khan, A. Asghar Esmailpour, A. Jalili, M. Lim, A. Tricoli, R.-S. Liu, X. Lu, E. Lovell and R. Amal, *Energy Environ. Sci.*, 2021, **14**, 3588-3598.
41. Q. Hu, Y. Qin, X. Wang, Z. Wang, X. Huang, H. Zheng, K. Gao, H. Yang, P. Zhang, M. Shao and C. He, *Energy Environ. Sci.*, 2021, **14**, 4989-4997.
42. D. Reyter, D. Bélanger and L. Roué, *Electrochim. Acta*, 2008, **53**, 5977-5984.
43. T. Zhu, Q. Chen, P. Liao, W. Duan, S. Liang, Z. Yan and C. Feng, *Small*, 2020, **16**, 2004526.
44. Y. Wang, A. Xu, Z. Wang, L. Huang, J. Li, F. Li, J. Wicks, M. Luo, D. H. Nam, C. S. Tan, Y. Ding, J. Wu, Y. Lum, C. T. Dinh, D. Sinton, G. Zheng and E. H. Sargent, *J Am Chem Soc*, 2020, **142**, 5702-5708.
45. N. C. Kani, J. A. Gauthier, A. Prajapati, J. Edgington, I. Bordawekar, W. Shields, M. Shields, L. C. Seitz, A. R. Singh and M. R. Singh, *Energy Environ. Sci.*, 2021, **14**, 6349-6359.
46. L. T. Roling, T. S. Choksi and F. Abild-Pedersen, *Nanoscale*, 2019, **11**, 4438-4452.
47. N. Yang, D. Chen, P. Cui, T. Lu, H. Liu, C. Hu, L. Xu and J. Yang, *SmartMat*, 2021, **2**, 234-245.
48. J. Gootzen, L. Lefferts and J. Van Veen, *Appl. Catal., A*, 1999, **188**, 127-136.
49. R. Jia, Y. Wang, C. Wang, Y. Ling, Y. Yu and B. Zhang, *ACS Catal.*, 2020, **10**, 3533-3540.
50. Y. Li, Y. K. Go, H. Ooka, D. He, F. Jin, S. H. Kim and R. Nakamura, *Angew Chem Int Ed Engl*, 2020, **59**, 9744-9750.
51. W. Wang and E. C. Tse, *Eur. J. Inorg. Chem.*, 2022, **2022**, e202200291.
52. M. Fang, X. Gao, J. Liang, B. Guo, L. Zou, J. Lu, Y. Gao, C. Edmund and J. Liu, *J. Mater. Chem. A*, 2022, **10**, 7013-7019.
53. J. Liang, X. Gao, B. Guo, Y. Ding, J. Yan, Z. Guo, E. C. Tse and J. Liu, *Angew. Chem. Int. Ed.*, 2021, **60**, 12770-12774.
54. Z. R. Ramadhan, A. R. Poerwoprajitno, S. Cheong, R. F. Webster, P. V. Kumar, S. Cychy, L. Gloag, T. M. Benedetti, C. E. Marjo and M. Muhler, *J. Am. Chem. Soc.*, 2022, **144**, 11094-11098.

55. A. Birrozzi, R. Belchi, J. Bouclé, D. Geiger, U. Kaiser, S. Passerini, N. Herlin-Boime and D. Bresser, *Energy Technology*, 2021, **9**, 2001067.
56. A. P. Haring, A. U. Khan, G. Liu and B. N. Johnson, *Adv. Opt. Mater.*, 2017, **5**, 1700367.
57. E. C. M. Tse, C. J. Barile, Y. Li, S. C. Zimmerman, A. Hosseini and A. A. Gewirth, *PCCP*, 2017, **19**, 7086-7093.
58. H. Xu, C. Shan, X. Wu, M. Sun, B. Huang, Y. Tang and C.-H. Yan, *Energy Environ. Sci.*, 2020, **13**, 2949-2956.
59. F. Song and X. Hu, *J. Am. Chem. Soc.*, 2014, **136**, 16481-16484.
60. S. Lee, L. Bai and X. Hu, *Angewandte Chemie*, 2020, **132**, 8149-8154.
61. Q. Wu, A. Olafsen, Ø. B. Vistad, J. Roots and P. Norby, *J. Mater. Chem.*, 2005, **15**, 4695-4700.
62. L. Lv, Z. Yang, K. Chen, C. Wang and Y. Xiong, *Adv. Energy Mater.*, 2019, **9**, 1803358.
63. R. Xie, G. Fan, L. Yang and F. Li, *ChemCatChem*, 2016, **8**, 363-371.
64. E. C. Tse, D. Schilter, D. L. Gray, T. B. Rauchfuss and A. A. Gewirth, *Inorg. Chem.*, 2014, **53**, 8505-8516.
65. E. C. Tse and A. A. Gewirth, *The Journal of Physical Chemistry A*, 2015, **119**, 1246-1255.
66. X. Mo, K. Chan and E. C. Tse, *Chem. Mater.*, 2019, **31**, 8230-8238.
67. D. Li, X. Wang, X. Mo, E. Tse and X. Cui, *Nat. Commun.*, 2022, **13**, 1-7.
68. N. M. Tzollas, G. A. Zachariadis, A. N. Anthemidis and J. A. Stratis, *Int. J. Environ. Anal. Chem.*, 2010, **90**, 115-126.
69. P. E. Blöchl, *Physical review B*, 1994, **50**, 17953.
70. G. Kresse and J. Furthmüller, *Physical review B*, 1996, **54**, 11169.
71. J. P. Perdew, K. Burke and M. Ernzerhof, *Phys. Rev. Lett.*, 1996, **77**, 3865.
72. M. Bajdich, M. García-Mota, A. Vojvodic, J. K. Nørskov and A. T. Bell, *J. Am. Chem. Soc.*, 2013, **135**, 13521-13530.
73. M. Garcia-Mota, M. Bajdich, V. Viswanathan, A. Vojvodic, A. T. Bell and J. K. Nørskov, *The Journal of Physical Chemistry C*, 2012, **116**, 21077-21082.
74. *Catal. Sci. Technol.*, 2014.
75. Y.-T. Kim and T. Mitani, *Journal of Catalysis*, 2006, **238**, 394-401.
76. Y. Levieux-Souid, J. f. Martin, P. Moreau, N. Herlin-Boime and S. Le Caër, *Small Methods*, 2022, **6**, 2200712.
77. M. A. Hasnat, J. A. Safwan, M. Rashed, Z. Rahman, M. M. Rahman, Y. Nagao and A. M. Asiri, *RSC Adv.*, 2016, **6**, 11609-11617.